

RoDiF: Robust Direct Fine-Tuning of Diffusion Policies with Corrupted Human Feedback

Amitesh Vatsa¹ Zhixian Xie¹ Wanxin Jin¹

Abstract

Diffusion policies are a powerful paradigm for robotic control, but fine-tuning them with human preferences is fundamentally challenged by the multi-step structure of the denoising process. To overcome this, we introduce a Unified Markov Decision Process (MDP) formulation that coherently integrates the diffusion denoising chain with environmental dynamics, enabling reward-free Direct Preference Optimization (DPO) for diffusion policies. Building on this formulation, we propose *RoDiF* (Robust Direct Fine-Tuning), a method that explicitly addresses corrupted human preferences. *RoDiF* reinterprets the DPO objective through a geometric hypothesis-cutting perspective and employs a conservative cutting strategy to achieve robustness without assuming any specific noise distribution. Extensive experiments on long-horizon manipulation tasks show that *RoDiF* consistently outperforms state-of-the-art baselines, effectively steering pretrained diffusion policies of diverse architectures to human-preferred modes, while maintaining strong performance even under 30% corrupted preference labels.

1. Introduction

Diffusion models have recently emerged as a compelling class of policies for robotic control (Ho et al., 2020; Chi et al., 2025), demonstrating superior capability in capturing multi-modal distributions and handling high-dimensional action spaces compared to traditional Gaussian or deterministic policies (Chi et al., 2025). While Behavior Cloning (BC) with diffusion models excels at many complex robot behaviors, such as contact-rich manipulation (Wolf et al., 2025) and locomotion (Yuan et al., 2025), the obtained diffusion policies are fundamentally limited by the quality

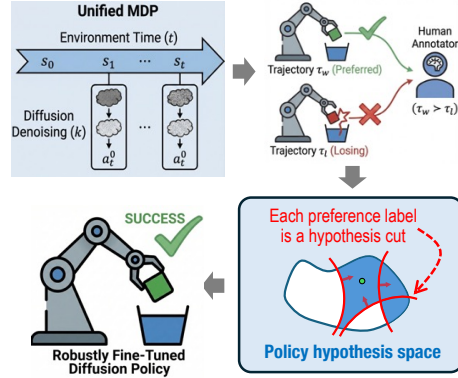


Figure 1. Overview of RoDiF. We introduce a Unified MDP to model the rollout of a diffusion policy, where human preferences are defined over trajectories in this unified decision process. To address noisy human feedback, RoDiF reinterprets the DPO objective through a geometric hypothesis-cutting perspective and adopts a conservative cutting strategy, enabling robust direct fine-tuning of diffusion policies.

of the training data. To enable robots to improve beyond their demonstrations or align with task/user specifics, it is necessary to fine-tune these policies using feedback signals.

Reinforcement Learning (RL) offers a pathway for such fine-tuning, but typically requires dense, well-engineered reward functions (Ma et al., 2025; Ren et al., 2024), which are notoriously difficult to specify for complex tasks (Tan et al., 2025). Consequently, preference-based reinforcement learning (PbRL) (Abdelkareem et al., 2022) has gained traction as an alternative, allowing agents to optimize behavior based on comparative feedback (e.g., $A \succ B$) rather than scalar rewards. In the domain of Large Language Models, Direct Preference Optimization (DPO) (Rafailov et al., 2023) has established a new paradigm by deriving a closed-form objective that optimizes the policy directly against preferences, bypassing the need for an explicit reward model.

However, extending DPO-style objectives to robotic diffusion policies presents a non-trivial theoretical challenge due to a structural mismatch in the generation process. Unlike autoregressive language models, a diffusion policy operates via a multi-step denoising chain nested within the environmental MDP. Existing preference optimization methods do not natively account for this dual temporal structure—where optimization must occur over the internal denoising steps

¹Intelligent Robotics and Interactive Systems (IRIS) Lab, Arizona State University, Tempe AZ, USA.
Emails: amitesh.vatsa.cd.mec20@iitbhu.ac.in, zxxie@asu.edu, wanxin.jin@asu.edu.

while respecting the external environmental dynamics. Furthermore, human feedback in robotic control is stochastic and often contains *model-mismatched* inconsistencies (e.g., occasional label flips, annotator disagreement, or nonstationary criteria) beyond the standard Bradley–Terry noise assumption. Naively fine-tuning on such data can overfit to conflicting comparisons, effectively optimizing to satisfy erroneous constraints rather than the underlying human intent, which degrades both alignment and task performance.

In this work, we propose **RoDiF** (Robust Direct Fine-Tuning), a framework to fine-tune pre-trained diffusion policies with noisy human preferences. We use a *Unified MDP* formulation that treats the diffusion denoising steps and environmental transitions as one decision process, enabling the derivation of a tractable DPO objective for diffusion policies. To address the challenge of label noise, we reformulate the optimization objective through the geometric lens of *hypothesis cutting*. By adopting a conservative cutting strategy, we derive a robust loss function that effectively ignoring the inconsistent feedback without requiring prior knowledge of noise distribution. Our contributions are:

- We propose a **Unified MDP** formulation that integrates the diffusion denoising process with environmental dynamics, enabling direct preference optimization for diffusion policies without explicit reward modeling.
- We introduce **RoDiF**, a geometrically grounded algorithm that robustly fine-tunes diffusion policies by leveraging conservative hypothesis cutting while mitigating the impact of inconsistency preference labels.
- We empirically demonstrate that RoDiF significantly outperforms existing baselines across diverse diffusion backbones on high-dimensional, long-horizon manipulation tasks, maintaining high alignment performance even under 30% corrupted preference labels.

2. Related Work

2.1. Preference Based Policy Learning

Reward-Based Methods A common approach to learning policies from human preferences is to first infer a reward model from human preferences and then optimize a policy using RL (Christiano et al., 2017) or trajectory optimization (Jin et al., 2022). Early works adopted active learning (Settles, 2012), while are largely limited to linear reward parameterization. Recent PbRL methods leverage neural networks to learn expressive reward models (Lee et al., 2021b; Park et al., 2022; Liang et al., 2022; Liu et al., 2022; Seneviratne et al., 2025), by modeling preferences probabilistically (e.g., Bradley–Terry (Bradley & Terry, 1952) or Plackett–Luce (Plackett, 1975)). In contrast, our method bypasses reward learning and directly fine-tunes diffusion policies from human preferences, leading to simpler implementation.

Reward-Free Methods To reduce computational overhead and improve efficiency, recent work (An et al., 2023;

Rafailov et al., 2023; Hejna & Sadigh, 2023; Hejna et al., 2024; Luu et al., 2025; Xia et al.) explores direct policy learning from human preferences without explicitly learning reward models. These methods re-parameterize action values with policy-dependent embeddings, enabling policies to be optimized directly from preference labels. Representative approaches include Direct Preference Optimization (DPO) (Rafailov et al., 2023) and its extensions (e.g., CPO (Xu et al., 2024b) and SimPO (Meng et al., 2024a) to reduce computation cost, IPO (Azar et al., 2024) to reduce overfitting), which directly optimize policies under preference supervision. Our method also builds on this paradigm but through formulating sequential denoising steps and environment interactions within a unified MDP.

2.2. Robust Preference Learning

A key challenge in preference-based policy learning is the inherent noise in human preference data. To address this issue, recent robust PbRL methods employ techniques such as data filtering (Cheng et al., 2024; Li et al., 2024; Huang et al., 2025), data augmentation (Heo et al., 2025), network architecture design (Xue et al., 2024), and hypothesis space cutting (Xie et al., 2025) to learn reliably from imperfect feedback. Robust preference-based learning has also been extended to reward-free settings: works such as (Ramesh et al., 2024; Kim et al., 2025; Cao et al., 2025) adopt conservative variants of the Direct Preference Optimization (DPO) loss to mitigate overfitting to noisy labels. Our method introduces a novel geometry-inspired robust objective based on hypothesis space cutting (Xie et al., 2025), enabling stable fine-tuning under noisy human preferences.

2.3. Diffusion Policy and its Fine-Tuning

Diffusion policies (Chi et al., 2025; Ze et al., 2024; Xue et al., 2025) achieve strong performance in robotic control but are typically trained via behavioral cloning, limiting their ability to improve beyond demonstration data. Recent work, such as DDPO (Black et al., 2023) and D3PO (Yang et al., 2023), formulates the diffusion denoising process as a sequential decision problem and extends Direct Preference Optimization (Rafailov et al., 2023) to enable post-learning refinement. However, these approaches focus on a static problem setting (e.g. image generation) and do not explicitly incorporate interactions with the physical environment.

When fine-tuning diffusion policies (Ma et al., 2025; Ren et al., 2024; Chen et al., 2025; Shan et al., 2024), an additional layer of sequential decision-making arises from environment dynamics. DPPO (Ren et al., 2024) and RSM (Ma et al., 2025) addresses this by applying reinforcement learning with explicit rewards, while FDPP (Chen et al., 2025) extends this framework to reward-based fine-tuning from human preferences. In contrast, FKPD (Shan et al., 2024) enables reward-free fine-tuning via KL regularization and ELBO-based approximations; however, these approxi-

mations inevitably introduce estimation bias. Our method achieves DPO-style fine-tuning, but jointly leveraging the full denoising trajectory and perform direct factorization to calculate the likelihood of the action. This eliminates the need for objective approximations and reduces the bias.

3. Preliminaries

3.1. Diffusion Policy

Diffusion policies (Chi et al., 2025; Ze et al., 2024; Xue et al., 2025) model action chunk generation as a sequential denoising process, built on diffusion probabilistic models (Ho et al., 2020). Conditioned on a system state observation \mathbf{s} , the policy starts from a noise distribution $\mathbf{a}^K \sim \mathcal{N}(\mathbf{0}, \mathbf{I})$ and iteratively refines a noisy action sequence through a fixed K number of denoising steps parameterized by θ :

$$\begin{aligned} \mathbf{a}^{k-1} &\sim p_\theta(\mathbf{a}^{k-1} | \mathbf{a}^k, \mathbf{s}), \\ p_\theta &\triangleq \mathcal{N}(\mathbf{a}^{k-1}; \boldsymbol{\mu}_k(\mathbf{a}^k, \epsilon_\theta(\mathbf{a}^k, k, \mathbf{s})), \boldsymbol{\Sigma}_k), \end{aligned} \quad (1)$$

where $k = K, K-1, \dots, 1$ is the step index, $\epsilon_\theta(\cdot)$ denotes a neural noise predictor, $\boldsymbol{\mu}_k(\cdot)$ is the denoising operator, and $\boldsymbol{\Sigma}_k$ is the step-dependent variance. Diffusion policies are typically learned via imitation learning by fitting $\epsilon_\theta(\cdot)$ to the injected noise in expert demonstrations. This class of policies is particularly effective at modeling complex, multi-modal action distributions (Wolf et al., 2025).

3.2. Bradley-Terry Preference Model

The Bradley-Terry model (Bradley & Terry, 1952) is a probabilistic formulation to model human pairwise preferences. Given two options a and b with utility scores $u_a, u_b \in \mathbb{R}$, the probability that human prefers a over b is defined as

$$\mathbb{P}(a \succ b) = \frac{\exp(u_a)}{\exp(u_a) + \exp(u_b)}. \quad (2)$$

In preference-based learning (Abdelkareem et al., 2022), items typically correspond to agent trajectories or state-action pairs, and the utility score u is parameterized by a reward- or policy-dependent function.

3.3. Unified Diffusion-Policy MDP Formulation

We consider a diffusion policy (Section 3.1) acting on an environment MDP, $\mathcal{M}_{\text{env}} = (\mathcal{S}_{\text{env}}, \mathcal{A}_{\text{env}}, P_{\text{env}}, R_{\text{env}}, \rho_{\text{env}})$. Here, $\mathbf{s} \in \mathcal{S}_{\text{env}}$, $\mathbf{a} \in \mathcal{A}_{\text{env}}$, $\mathbf{s}_0 \in \rho_{\text{env}}$, $P_{\text{env}}(\mathbf{s}_{t+1} | \mathbf{s}_t, \mathbf{a}_t)$, and $R_{\text{env}}(\mathbf{s}_t, \mathbf{a}_t)$ are the environment state, action, initial state, transition, and reward, respectively.

As a notation convention, we denote the denoising step inside the diffusion policy by the inverse-time index k (superscript) and the environment rollout step by t (subscript). At the environment state \mathbf{s}_t at rollout time t , the denoising process within the diffusion policy is modeled as a Markov Chain $(\mathbf{a}_t^K, \mathbf{a}_t^{K-1}, \dots, \mathbf{a}_t^0)$ over a horizon of $K+1$ steps (Black et al., 2024), where \mathbf{a}_t^k represents the denoising

state at the denoising step k . This denoising chain is conditioned on the environment state \mathbf{s}_t and evolves following the reverse denoising process $p_\theta(\mathbf{a}_t^{k-1} | \mathbf{a}_t^k, \mathbf{s}_t)$ parameterized by θ in (Eq. 1), with drawing a random $\mathbf{a}_t^K \sim \mathcal{N}(\mathbf{0}, \mathbf{I})$. The environment MDP evolves according to the trajectory $(\mathbf{s}_0, \mathbf{a}_0, \mathbf{s}_1, \mathbf{a}_1, \dots, \mathbf{s}_t, \mathbf{a}_t, \dots)$, where each action \mathbf{a}_t corresponds to the final denoising state of the corresponding diffusion process, i.e., $\mathbf{a}_t = \mathbf{a}_t^0$.

We employ a Unified MDP formulation to integrate both the diffusion denoising process and the environment rollout process. Specifically, we define the Unified MDP as a tuple $\mathcal{M}_{\text{unified}} = (\mathcal{S}^+, \mathcal{A}^+, P^+, R^+, \rho_0^+)$. The unified system state $\mathbf{s}^+ \in \mathcal{S}^+$ and action $\mathbf{a}^+ \in \mathcal{A}^+$ are defined as:

$$\begin{aligned} \mathbf{s}^+ &\triangleq (\mathbf{a}_t^K, \mathbf{s}_t) \\ \mathbf{a}^+ &\triangleq (\mathbf{a}_t^{K-1}, \mathbf{a}_t^{K-2}, \dots, \mathbf{a}_t^0) \end{aligned} \quad (3)$$

The reward is defined as:

$$R^+(\mathbf{s}^+, \mathbf{a}^+) \triangleq R_{\text{env}}(\mathbf{s}_t, \mathbf{a}_t) = R_{\text{env}}(\mathbf{s}_t, \mathbf{a}_t^0) \quad (4)$$

The transition of this flattened MDP is defined as

$$P^+(\mathbf{s}_{t+1}^+ | \mathbf{s}_t^+, \mathbf{a}_t^+) \triangleq \mathcal{N}(0, \mathbf{I}) \otimes P_{\text{env}}(\mathbf{s}_{t+1} | \mathbf{s}_t, \mathbf{a}_t^0) \quad (5)$$

with the initial state distribution $\rho^+ \triangleq \mathcal{N}(0, \mathbf{I}) \otimes \rho_{\text{env}}$.

Under the above formulation of Unified MDP, we define its policy for the Unified MDP as $\pi(\mathbf{a}_t^+ | \mathbf{s}_t^+)$. Based on the definition in (Eq. 3) and also the Markov properties of the denoising chain (Black et al., 2024), we have the following factorization of the Unified-MDP policy

$$\pi_\theta(\mathbf{a}_t^+ | \mathbf{s}_t^+) = \prod_{k=1}^K p_\theta(\mathbf{a}_t^{k-1} | \mathbf{a}_t^k, \mathbf{s}_t). \quad (6)$$

where $p_\theta(\mathbf{a}^{k-1} | \mathbf{a}^k, \mathbf{s})$ is defined in (1).

3.4. DPO with Unified MDP

Under the Unified MDP formulation, we consider optimizing the policy π given an optimal state-action value function $Q^*(\mathbf{s}^+, \mathbf{a}^+)$ corresponding to the *unknown* reward R^+ in (4). We define our objective as

$$\max_{\pi} \mathbb{E}_{\substack{\mathbf{s}^+ \sim d^{\pi} \\ \mathbf{a}^+ \sim \pi(\cdot | \mathbf{s}^+)}} Q^*(\mathbf{s}^+, \mathbf{a}^+) - \beta \text{KL}(\pi || \pi_{\text{ref}}) \quad (7)$$

where $\pi_{\text{ref}}(\mathbf{a}^+ | \mathbf{s}^+)$ is a reference policy for the unified MDP. The above objective means that the policy needs to be fine-tuned to maximize the value of Q^* , while a regularization term $-\beta \text{KL}(\pi || \pi_{\text{ref}})$ prevents drifting away from the reference policy π_{ref} . $\beta > 0$ controls the regularization strength.

Following (Peters & Schaal, 2007; Peng et al., 2019), (7) permits a closed-form optimal policy given an Q^* function.

$$\pi^*(\mathbf{a}^+ | \mathbf{s}^+) = \frac{1}{Z(\mathbf{s}^+)} \pi_{\text{ref}}(\mathbf{a}^+ | \mathbf{s}^+) \exp\left(\frac{1}{\beta} Q^*(\mathbf{s}^+, \mathbf{a}^+)\right), \quad (8)$$

where Q^* is the given optimal state-action value function and $Z(s^+)$ is the partition function.

Rearranging Eq. (8), we can express the optimal Q^* purely in terms of the likelihood ratio between the optimal policy and the reference policy:

$$Q^*(s^+, a^+) = \beta \log \frac{\pi^*(a^+|s^+)}{\pi_{\text{ref}}(a^+|s^+)} + \beta \log Z(s^+). \quad (9)$$

The above equation is a critical reparameterization trick (Rafailov et al., 2023) in the following preference optimization: the policy itself can be used to express a corresponding state-action value, eliminating the need to approximating or compute Q^* itself.

3.4.1. ADVANTAGE BRADLEY-TERRY PREFERENCE

Typically, Bradley-Terry preference model (2) is defined on the reward function R^+ . However, such models have been shown to be inconsistent with real human preferences (Knox et al., 2024): for instance, consider a sparse goal-reaching reward. Two segments that do not reach the goal would have the same returns even if one moved towards the goal while the other moved away from it. Thus, we follow (Knox et al., 2024; Hejna et al., 2023) and choose per-step advantage function for the human preference model.

Specifically, define the human’s implicit state-action value function $Q^*(s^+, a^+)$ and value function $V^*(s^+)$. Human’s implicit advantage function is defined as $A^*(s^+, a^+) \triangleq Q^*(s^+, a^+) - V^*(s^+)$. Consider two actions (a_w^+, a_l^+) drawn from policy $\pi(\cdot|s^+)$. The human ranks the two actions as $(a_w^+|s^+ \succ a_l^+|s^+)$, i.e., a_w^+ is preferred than a_l^+ , according to the probability

$$P(a_w^+|s^+ \succ a_l^+|s^+) = \frac{e^{A^*(a_w^+, s^+)/\alpha}}{e^{A^*(a_w^+, s^+)/\alpha} + e^{A^*(a_l^+, s^+)/\alpha}} \quad (10)$$

where $\alpha > 0$ is the temperature parameter for the Boltzmann distribution (intuitively, the human rationality). By simplification, the above (10) can be reduced to

$$\begin{aligned} P(a_w^+|s^+ \succ a_l^+|s^+) &= \sigma_\alpha(\Delta Q^*(a_w^+|s^+, a_l^+|s^+)) \\ \Delta Q^*(a_w^+|s^+, a_l^+|s^+) &\triangleq Q^*(s^+, a_w^+) - Q^*(s^+, a_l^+). \end{aligned} \quad (11)$$

We use the action-value function Q^* rather than the advantage function A^* in (11), since the state-value term $V^*(s^+)$ cancels out when taking differences between advantages.

3.4.2. PER-CONTROL DPO FOR DIFFUSION POLICIES

Under the reparameterization trick in (9), we can parameterize the unknown human Q^* function in (11) with the parametrized policy π_θ . Also, considering the definition and Markov property of the diffusion policy π_θ in (6) in the Unified MDP, we have

$$\begin{aligned} \Delta Q_\theta(a_w^+|s^+, a_l^+|s^+) &= \beta \sum_{k=1}^K \log \frac{p_\theta(a_w^{k-1}|a_w^k, s)}{\pi_{\text{ref}}(a_w^{k-1}|a_w^k, s)} \\ &\quad - \beta \sum_{k=1}^K \log \frac{p_\theta(a_l^{k-1}|a_l^k, s)}{\pi_{\text{ref}}(a_l^{k-1}|a_l^k, s)}, \end{aligned} \quad (12)$$

Thus, given a dataset of human preference labels for per-control of diffusion policy $\mathcal{D} = \{(a_{i,w}^+|s_i^+ \succ a_{i,l}^+|s_i^+)\}_{i=1}^N$ the DPO objective for fine-tuning the diffusion policy policy π_θ can be formulated as maximizing the likelihood (Rafailov et al., 2023) of the advantage preference probabilities (11):

$$\mathcal{L}_{\text{DPO}}(\theta) = - \sum_{i=1}^N \log \sigma_\alpha(\Delta Q_\theta(a_{i,w}^+|s_i^+, a_{i,l}^+|s_i^+)). \quad (13)$$

3.4.3. EXTENSION TO TRAJECTORY COMPARISON

While the above DPO formulation of per-control preference has nice theoretical meaning, but it can be incontinent for practice because providing per-control preference labels \mathcal{D} can be labor-consuming for human users. Instead, it’s more viable for human users to provide per-trajectory/episode preference labels. Suppose a diffusion policy π_θ generates two trajectories that are compared by a human observer, denoted as $(\tau_w \succ \tau_l)$, where τ_w and τ_l represent the winning (preferred) and losing (not preferred) trajectories, respectively. We can leverage the assumption: if a trajectory τ_w is preferred over τ_l , then every constituent state-action pair $(s_{t,w}^+, a_{t,w}^+)$ in the winning trajectory τ_w is likely superior to the corresponding pair $(s_{t,l}^+, a_{t,l}^+)$ in τ_l . Accordingly, for preference label of a pair (τ_w, τ_l) of trajectories of length T , we perform T comparisons of $\Delta Q_\theta(a_{t,w}^+|s_{t,w}^+, a_{t,l}^+|s_{t,l}^+)$ and compute the total loss

$$\mathcal{L}(\theta, \tau_w \succ \tau_l) \triangleq - \sum_{t=0}^{T-1} \log \sigma_\alpha(\Delta Q_\theta(a_{t,w}^+|s_{t,w}^+, a_{t,l}^+|s_{t,l}^+)) \quad (14)$$

Given M trajectory pairs, the per-control diffusion policy DPO loss (13) can be extended into

$$\mathcal{L}_{\text{DP-DPO}}(\theta) \triangleq \sum_{i=1}^M \mathcal{L}(\theta, \tau_w^{(i)} \succ \tau_l^{(i)}) \quad (15)$$

4. Robust Direct Fine-Tuning

The standard DPO formulation assumes preferences derive from a single Bradley-Terry model. While this captures intrinsic ambiguity, it fails to account for model-mismatched inconsistencies, such as label flips or annotator errors, which we term **corrupted preference labels**. Since these out-of-distribution labels render optimization brittle (Lee et al., 2021a), we propose a fine-tuning objective robust to such corruption without assuming a known corruption data distribution.

4.1. Interpreting DPO Objective as Hypothesis Cutting

Let Θ be the entire hypothesis space for the parameterized diffusion policies (6). Define $\theta^H \in \Theta$ the true diffusion policy parameter aligned with human preferences. Based on the reparameterization in (12), $\Delta Q_{\theta^H} = \Delta Q^*$ in (11).

In (11), if we let the temperature $\alpha \rightarrow 0$, $\sigma_\alpha(\cdot)$ will become the Heaviside step function $\mathbf{H}(\cdot)$, and Bradley-Terry model becomes

$$P(\mathbf{a}_w^+ | \mathbf{s}^+ \succ \mathbf{a}_l^+ | \mathbf{s}^+) = \begin{cases} 1 & \Delta Q^*(\mathbf{a}_w^+ | \mathbf{s}^+, \mathbf{a}_l^+ | \mathbf{s}^+) \geq 0 \\ 0 & \text{otherwise} \end{cases} \quad (16)$$

Due to $\Delta Q_{\theta^H} = \Delta Q^*$, we can interpret from (16) that each human preference pair $(\mathbf{a}_{i,w}^+ | \mathbf{s}_i^+ \succ \mathbf{a}_{i,l}^+ | \mathbf{s}_i^+)$ will induce an inequality constraint \mathcal{C}_i on the policy parameter θ :

$$\mathcal{C}_i \triangleq \left\{ \theta \in \Theta \mid \Delta Q_\theta(\mathbf{a}_{i,w}^+ | \mathbf{s}_i^+, \mathbf{a}_{i,l}^+ | \mathbf{s}_i^+) \geq 0 \right\} \quad (17)$$

and the true policy parameter $\theta^H \in \mathcal{C}_i$.

In another perspective, as in Fig. 2 (left), \mathcal{C}_i can be interpreted as a **cut** of the hypothesis space Θ , removing the hypothesis space portion which does not contain θ^H . In this geometry interpretation, $\sigma_{\alpha \rightarrow 0}(\Delta Q_\theta) = \mathbf{H}(\Delta Q_\theta)$ becomes an indicator function of the cut \mathcal{C}_i ,

$$\mathbf{H}(\Delta Q_\theta(\mathbf{a}_{i,w}^+ | \mathbf{s}_i^+, \mathbf{a}_{i,l}^+ | \mathbf{s}_i^+)) = \begin{cases} 1 & \theta \in \mathcal{C}_i \\ 0 & \text{else} \end{cases} \quad (18)$$

Therefore, the diffusion policy DPO loss (13) equivalent to

$$\max_{\theta} \prod_{i=1}^N \mathbf{H}(\Delta Q_\theta(\mathbf{a}_{i,w}^+ | \mathbf{s}_i^+, \mathbf{a}_{i,l}^+ | \mathbf{s}_i^+)), \quad (19)$$

where the product of indicator functions is equivalent to taking the intersection of all preference-induced cuts \mathcal{C}_i , $i = 1, 2, \dots, N$. As more cuts are applied, the interacting hypothesis space gets progressively *shrunk*, eventually, we can retain θ^H from the shrinking intersection set $\theta^H \in \Theta \cap \mathcal{C}_1 \cap \mathcal{C}_2 \dots \cap \mathcal{C}_N$.

4.2. Robust Direct Fine-Tuning Objective

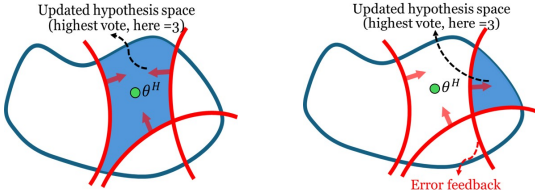


Figure 2. Illustration of intersecting all induced cuts. Left: all three preferences are consistent with (16). The aligned parameter θ^H falls into the intersection. Right: In case of one corrupted preference, the updated hypothesis space does not contain θ^H .

Human preference labels can be inherently inconsistent, e.g., $(\mathbf{a}_w^+ | \mathbf{s}^+ \succ \mathbf{a}_l^+ | \mathbf{s}^+)$ is labeled as $(\mathbf{a}_w^+ | \mathbf{s}^+ \prec \mathbf{a}_l^+ | \mathbf{s}^+)$, due to factors such as fatigue/errors, disagreement across

annotators, or nonstationary criteria over time. Thus, in the following we will develop a robust mechanism based on the above geometric interpretation of hypothesis cutting.

To proceed, we view each $\mathbf{H}(\Delta Q_\theta(\cdot, \cdot))$ in (18) as a voting function over the hypothesis space: Among the hypotheses in Θ , θ s that satisfy the cut \mathcal{C}_i in (17) receive “+1” vote, since $\mathbf{H}(\Delta Q_\theta(\cdot, \cdot))$ outputs 1. In contrast, parameters that violate the cut receive “0” vote. We use $V_{\mathcal{C}_i}(\theta)$ to denote the vote generated by i -th cut \mathcal{C}_i (17):

$$V_{\mathcal{C}_i}(\theta) \triangleq \mathbf{H}(\Delta Q_\theta(\mathbf{a}_{i,w}^+ | \mathbf{s}_i^+, \mathbf{a}_{i,l}^+ | \mathbf{s}_i^+)) \quad (20)$$

With this notation of the votes, the following lemma states an equivalent solution set to (19) and also the implication if the human preference label set contains corrupted labels.

Lemma 4.1. Consider a dataset of human preference labels $\mathcal{D} = \{(\mathbf{a}_{i,w}^+ | \mathbf{s}_i^+ \succ \mathbf{a}_{i,l}^+ | \mathbf{s}_i^+)\}_{i=1}^N$, and define θ^H as true diffusion policy parameter aligned with human preference. If all preference labels in \mathcal{D} is consistent with (16), then

$$\theta^H \in \arg \max_{\theta} \sum_{i=1}^N V_{\mathcal{C}_i}(\theta) \quad (21)$$

Otherwise when \mathcal{D} contain corrupted preference labels, i.e., $\exists j, \Delta Q^*(\mathbf{a}_{j,w}^+ | \mathbf{s}_j^+, \mathbf{a}_{j,l}^+ | \mathbf{s}_j^+) < 0$, then θ^H cannot be found in the above solution set.

Proof. The proof is given in Appendix A.1. \square
We explain the above lemma using Fig. 2 (right). Any corrupted preference label $(\mathbf{a}_{j,w}^+ | \mathbf{s}_j^+, \mathbf{a}_{j,l}^+ | \mathbf{s}_j^+)$ means that $\theta^H \notin \mathcal{C}_j$, i.e., the induced cut will exclude the true θ^H from the current hypothesis space. Once θ^H is removed, all subsequent updates operate on a restricted hypothesis space that no longer contains θ^H , demonstrating how a single incorrect preference can irreversibly derail the learning process.

To still robustly find the true policy θ^H under human corrupted preference label, we employ a conservative voting strategy. The intuitive idea is stated below. Reconsider the example in Fig. 2 (right), where three hypothesis cuts are made, one of which corresponds to corrupted preference label. If we pick the regions of greater or equal two votes, shown in Fig. 3, then we can still guarantee the remaining hypothesis space (blue region in Fig. 3) to contain θ^H .

Formally, we introduce a **conservativeness level** $\gamma \in [0, 1]$, which represents an estimated upper bound on the ratio of the corrupted labels, meaning that *at least* $\lfloor (1-\gamma)N \rfloor$ labels of given N preference labels satisfy (16). Then, we have the following lemma stating a robust loss, whose solution contains the true aligned diffusion policy parameter θ^H .

Lemma 4.2. Given a dataset of N human preference labels and a conservative level $\gamma \in (0, 1)$ for conservative estimate of actual label corruption rate, i.e. at least $\lfloor (1-\gamma)N \rfloor$ labels satisfy (16), the human-aligned diffusion policy parameter is the solution to the **robust direct fine-tuning loss** below

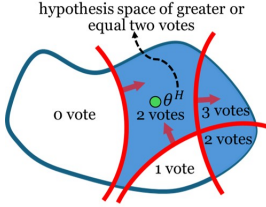


Figure 3. A conservative voting strategy to ensure robustness. By retaining only the hypotheses that receive at least two votes, the true policy parameter θ^H remains in the updated hypothesis space even when one out of three preferences is corrupted.

$$\theta^H \in \arg \max_{\theta} \mathbf{H} \left(\sum_{i=1}^N V_{C_i}(\theta) - \lfloor (1-\gamma)N \rfloor + 0.5 \right). \quad (22)$$

Proof. The proof is given in Appendix A.2. \square

Geometrically, the above direct fine-tuning loss relaxes the strict requirement of all consistent cuts: a parameter θ remains in the hypothesis space even if it violates a limited number of cuts. In particular, the policy is allowed to ignore up to γN corruption cuts, thereby mitigating catastrophic “false cuts” caused by a small fraction of corrupted labels. Specifically, if γ is chosen as zero, the solution set in (22) becomes the same as the one in (21), i.e., the corruption-free fine-tuning is a special case of robust fine-tuning.

4.3. Practical Loss for Robust Direct Fine-Tuning

To enable gradient-based optimization with the robust direct fine-tuning loss in (22), we soften the non-differentiable Heaviside step function \mathbf{H} in (20) and (22) using a sigmoid function $\sigma_\alpha(x) = \frac{1}{1+e^{-x/\alpha}}$ with temperature $\alpha > 0$.

For the trajectory pairs (recall Section 3.4.3), we have the dataset $\{(\tau_w^{(i)}, \tau_l^{(i)})\}_{i=1}^M$ with each trajectory of length T . Define the per-pair, per-step preference voting function (20) by softening \mathbf{H} using sigmoid function σ_α

$$\hat{V}_{C_{i,t}} \triangleq \sigma_\alpha \left(\Delta Q_\theta(\mathbf{a}_{i,t,w}^+ | \mathbf{s}_{i,t,w}^+, \mathbf{a}_{i,t,l}^+ | \mathbf{s}_{i,t,l}^+) \right), \quad (23)$$

for $i = 1, 2, \dots, M$, $t = 1, 2, \dots, T$, with ΔQ_θ defined using the reparameterization (12). A soften version of the robust direct fine-tuning loss (22) is defined

$$\mathcal{L}_{\text{RoDiF}}(\theta) = -\log \sigma_\alpha \left(\sum_{i=1}^M \sum_{t=1}^T \hat{V}_{C_{i,t}}(\theta) - \nu(1-\gamma)MT \right). \quad (24)$$

where $\nu \approx 1$ is a scaling factor which replaces the floor operation in (22).

5. Experiments

In experiment, we aim to answer the following questions: (1) **Alignment Effectiveness:** Can RoDiF effectively steer a pretrained multi-modal policy toward a preferred behavior without degrading the policy’s stability? (2) **Robustness to**

Noise: Does RoDiF maintain performance when the preference dataset contains different levels of corrupted labels? (3) **Architecture Agnosticism:** Is our method effective across different diffusion backbones?

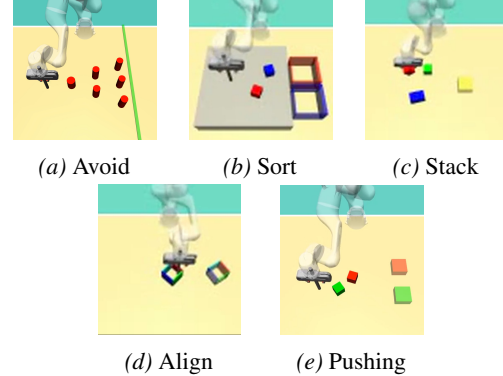


Figure 4. Five long-horizon manipulation tasks adapted from D3IL benchmark. (Jia et al., 2024)

5.1. Experimental Setup

Benchmark Tasks We evaluate our method on five long-horizon manipulation tasks adapted from *D3IL benchmark* (Jia et al., 2024), as shown in Fig. 4. The details of the five benchmark tasks are listed in Table 1 and in Appendix B.1.

Diffusion Policy Architectures We use three diffusion architectures (details in Appendix B.2): (1) **State-Based UNet** (*Avoid, Pushing*): Standard Conditional UNet (Chi et al., 2025) predicting action chunks from observation history. (2) **Transformer ACT** (*Sorting, Stacking*): Action Chunking Transformer (Zhao et al., 2023) utilizing ResNet-18 features for visual feature extraction. (3) **Image-Based MLP** (*Aligning*): Single-action diffusion using the same ResNet-18 visual backbone as above. The training settings of all policies in each task is shown in Appendix B.3.

Human Preference Label Generation We use a pairing strategy to generate human preference labels. We collected a set of N_{win} winner (preferred mode) trajectories and N_{lose} loser trajectories for each task. We construct the preference dataset $\mathcal{D}_{\text{pair}}$ by forming all possible Cartesian products of winners and losers. This results in a total dataset size of $N_{\text{pair}} = N_{\text{win}} \times N_{\text{lose}}$ (See numbers for each tasks in Appendix B.4). To generate corrupted data labels, we randomly select a portion of pairs from $\mathcal{D}_{\text{pref}}$. For these pairs, the preference labels are permanently inverted. This mimics real-world scenarios where a portion of the data is mislabeled due to annotator error or ambiguity.

Evaluation Metrics We assess the fine-tuned diffusion policies by analyzing the behavioral modes manifested during rollout episodes for each task. We report results using (1) **Mode Alignment Rate:** The percentage of trajectories that match the preferred mode (last col. of Table 1). (2) **Success Rate:** Percentage of episodes in which the robot successfully achieves the goal (second col. of Table 1).

Table 1. The setup of five D3IL Benchmark tasks (Jia et al., 2024) and our preference definition for each task.

| Task Name | Description (how to define success) | Observation space | Pretrained Behavior (Modes) | Mode Preference (Winner) |
|-----------|---|------------------------------------|-----------------------------|--------------------------|
| Avoid | reach finish line while avoiding obstacles | 4-dim (EE pos, goal) | Pass left or right | Left-side trajectory |
| Pushing | Push red and green blocks to matching targets | 10-dim (EE pose, block pos/orient) | Diverse sorting orders | Red-to-Red |
| Sorting | Sort red and blue blocks into matching boxes | (4 + 3X)-dim ($X = 2$ blocks) | Arbitrary sorting sequences | Red-then-Blue sequence |
| Align | Push hollow box to target pose | 2 × 96 × 96 RGB + Proprioception | Push from inside or outside | Push from Inside |
| Stacking | Stack three colored blocks into a tower | 2 × 96 × 96 RGB + Proprioception | 6 stacking permutations | Red → Blue → Green |

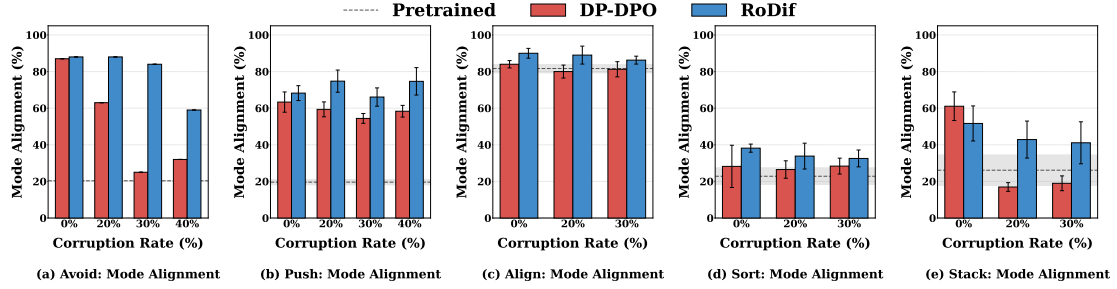


Figure 5. Mode alignment rate of the fine-tuned diffusion policies using RoDiF and DP-DPO under different corruption levels. DP-DPO utilizes the standard DPO loss (15) while keeping all other settings identical. For RoDiF, the hyperparameter settings were adapted based on the task characteristics. For the **Avoid** and **Push** tasks, we fixed $\alpha = 1$ and $\beta = 0.1$, while γ was set according to the noise level: $\gamma = 0$ for 0% noise, $\gamma = 0.3$ for 20% noise, $\gamma = 0.4$ for 30% noise, and $\gamma = 0.45$ for 40% noise. For the **Sort**, **Align** and **Stack** tasks, we utilized fixed hyperparameters across all noise levels: $\alpha = 1$, $\beta = 0.005$, and $\gamma = 0.45$.

5.2. Results

Overall Performance The overall results are reported in Table 2 and Fig. 5. In Table 2, we demonstrate the effectiveness of RoDiF for fine-tuning diffusion policy under different levels of preference label corruption. It shows that RoDiF consistently steers the policy toward the user-specified modes, demonstrating robust performance even in challenging scenarios. Specifically, for four tasks **Avoid**, **Pushing**, **Sorting**, and **Stacking**, the target behavior mode corresponds to a **non-dominant mode** of the pretrained policy (baseline alignment < 27%). In these cases, the method must override the policy’s strong natural tendency to execute alternative behaviors. Additional result and visualization is shown in Appendix C.

Table 2 also show that the success rates of the fine-tuned policies have slightly increased compared to the pretrained policies. This indicates that while steering the diffusion policy toward preferred mode, RoDiF does not compromise the overall task performance, **maintaining task stability throughout the fine-tuning process**. Furthermore, Table 2 demonstrates our method is effective across different diffusion backbones, validating its **architecture agnosticism**.

In Fig. 5, we compare the performance of RoDiF against the baseline DP-DPO, which utilizes the standard DPO loss (15) while keeping all other settings identical. The results demonstrate that under 0% label corruption, both methods fine-tune the policy with comparable performance. However, as the corruption rate increases, RoDiF demonstrates significantly greater robustness, maintaining high fine-tuning performance where the baseline DPO degrades.

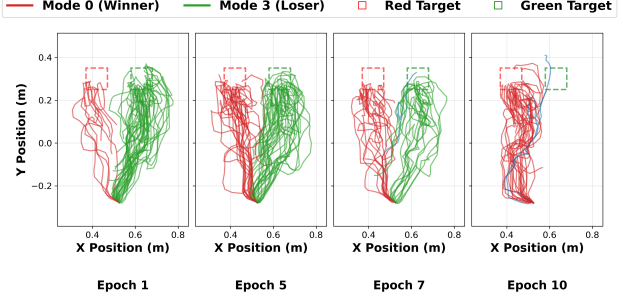


Figure 6. Visualizing behavior (policy rollouts) mode during fine-tuning in the pushing task.

Qualitative Results. Fig. 6 visualizes the evolution of the policy mode during fine-tuning for the *Pushing* task, where the objective is to steer towards a non-dominant mode. At Epoch 1, the rollout trajectories are heavily clustered around the dominant mode (visualized in green), reflecting the bias of the pretrained backbone. However, as training progresses, the distribution shifts significantly, with the target non-dominant trajectories (visualized in red) becoming prevalent by the final epoch.

We also validate RoDiF’s capability to reinforce **dominant modes**. For the *Avoid* task, when steered towards the already-preferred trajectory, the policy achieved a mode alignment of 84% over 100 evaluation rollouts as shown in Fig. 7, confirming it can sharpen existing

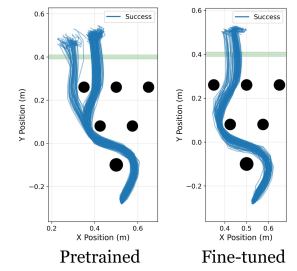


Figure 7. Mode visualization for avoid task

Table 2. Overall performance (success rate and mode alignment rate) of the diffusion policies fine-tuned by RoDiF under different label corruption rates. γ , β and α values follow the same setting in Fig. 5.

| Task | Backbone | PreTrained | | RoDiF (0% Corruption) | | RoDiF (20% Corruption) | | RoDiF (30% Corruption) | |
|----------|-------------|-------------------|-------------------|--------------------------------------|-------------------------------------|-------------------------------------|-------------------------------------|-------------------------------------|--------------------|
| | | Success | Alignment | Success | Alignment | Success | Alignment | Success | Alignment |
| Avoid | UNet | 78.00 \pm 0.00% | 20.33 \pm 0.00% | 88.00 \pm 0.00% | 88.00 \pm 0.00% | 86.00 \pm 0.00% | 86.00 \pm 0.00% | 84.00 \pm 0.00% | 84.00 \pm 0.00% |
| Pushing | UNet | 57.67 \pm 1.25% | 19.59 \pm 1.45% | 52.60 \pm 2.06% | 68.23 \pm 4.06% | 56.14 \pm 2.47% | 74.77 \pm 6.06% | 54.00 \pm 1.41% | 66.09 \pm 4.99% |
| Sorting | Transformer | 82.00 \pm 4.00% | 22.82 \pm 4.58% | 83.85 \pm 5.26% | 38.17 \pm 2.22% | 79.43 \pm 2.97% | 33.82 \pm 7.07% | 84.00 \pm 6.00% | 32.55 \pm 4.61% |
| Aligning | MLP | 5.00 \pm 3.54% | 81.67 \pm 2.36% | 12.00 \pm 5.10% | 90.00 \pm 2.67% | 8.33 \pm 4.71% | 89.00 \pm 4.90% | 8.33 \pm 4.71% | 86.25 \pm 2.17% |
| Stacking | Transformer | 23.03 \pm 2.27% | 26.12 \pm 8.34% | 28.75 \pm 12.44% | 51.66 \pm 9.57% | 25.00 \pm 10.80% | 42.86 \pm 10.10% | 27.00 \pm 6.00% | 41.09 \pm 11.47% |

behaviors as well.

Finally, we highlight the **sample efficiency** of our approach; for the *Pushing* task, RoDiF use as few as 10 winner-loser pairs was sufficient to achieve a mode alignment rate of 76% (see the visualization in Appendix C), significantly reducing the human preference annotation burden.

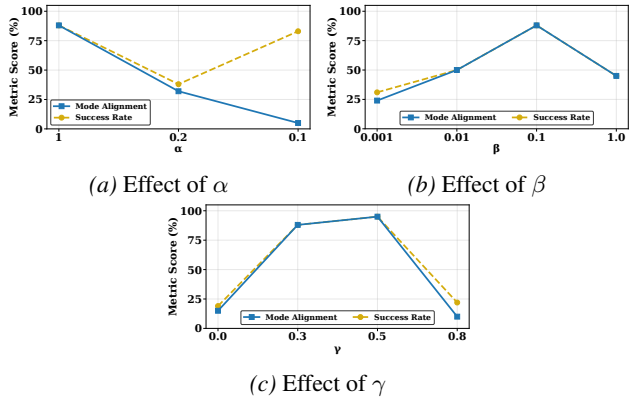


Figure 8. Ablation studies on the sensitivity of the success rate and mode alignment to variations in β , α , and γ .

5.3. Baseline Comparisons

Table 3 evaluates RoDiF against baselines under varying noise. Margin-based **SimPO** (Meng et al., 2024b) collapses under 20% noise (43% \rightarrow 10% success), confirming that hard margins overfit to systematic corruption. **CPO** (Xu et al., 2024a) remains stable (\sim 77% success) but fails to steer effectively (low alignment), likely constrained by its behavior cloning term. **IPO** (Azar et al., 2023) proves inconsistent. In contrast, **RoDiF** maintains robustness across all levels ($>84\%$ success). At 20% noise, RoDiF achieves **86% success**, outperforming the strongest baseline by +9 % and demonstrating that it effectively isolates the steering signal from systematic label noise.

Table 3. **Robustness Comparison.** Performance comparison of RoDiF against baseline preference optimization methods

| Method | Success Rate (%) | | | Mode Alignment (%) | | |
|--------|------------------|--------------|--------------|--------------------|--------------|--------------|
| | 0% | 20% corr. | 30% corr. | 0% corr. | 20% corr. | 30% corr. |
| RoDiF | 88.00 | 86.00 | 84.00 | 88.00 | 86.00 | 84.00 |
| CPO | 76.00 | 77.00 | 78.00 | 69.00 | 70.00 | 71.00 |
| IPO | 65.00 | 49.00 | 69.00 | 63.00 | 47.00 | 58.00 |
| SimPO | 43.00 | 10.00 | 27.00 | 43.00 | 9.00 | 21.00 |

5.4. Ablation Study

For the RoDiF method, we conducted a sensitivity analysis on the *Avoid* task under a fixed label corruption rate of 20%. We examined the impact of three hyperparameters: temperature α , KL weight β , and conservativeness level γ .

Temperature (α): Fig. 8a shows that a softer (high temperature) ($\alpha=1$) significantly outperforms a sharp one ($\alpha=0.1$). Low temperature α makes the voting function (20) near a binary step. This leads to *gradient vanish* for learning signals. In contrast, $\alpha = 1$ maintains necessary gradient flow, facilitating continuous optimization.

KL-Constraint (β): Fig. 8b reveals a trade-off governed by β . Large values ($\beta=1$) induce gradient saturation, causing the policy to become trapped in the pretrained mode. Conversely, very small β values lead to overly aggressive updates that degrade trajectory smoothness and leads to collision. Empirically, $\beta = 0.1$ provides the best balance for effective mode adaptation.

Conservativeness level (γ): γ is a conservative estimate of the actual corruption rate, which can be considered as the decision boundary for noise rejection. Given the actual corruption rate 20%, Fig. 8c shows that γ should match or slightly surpass the actual corruption rate for RoDiF to work. This corresponds to the theory in Lemma 4.2. At large levels like $\gamma = 0.8$, the RoDiF becomes overly conservative, discarding valid but imperfect trajectories.

6. Conclusion

In this work, we propose RoDiF, a novel framework for robust direct fine-tuning of diffusion policies under corrupted human feedback. RoDiF introduces a unified MDP that jointly models the diffusion denoising process and environment dynamics, enabling the application of Direct Policy Optimization (DPO) to diffusion policies. To address noisy preference feedback, RoDiF reinterprets the DPO objective through a geometric hypothesis-cutting perspective and adopts a conservative cutting strategy, resulting in robust policy fine-tuning. Across diverse robotic tasks, RoDiF matches the performance of state-of-the-art preference-based fine-tuning methods under clean data and significantly outperforms them when a large fraction of preferences is corrupted.

Impact Statement

This work advances the safety and reliability of preference-based robot learning by introducing a robust fine-tuning framework for diffusion policies under noisy human feedback. By explicitly mitigating the effects of erroneous or inconsistent preferences, the proposed approach reduces the risk of brittle or unstable policy updates, which is critical for deploying robotic systems in real-world, safety-sensitive environments. The ethical and societal implications of this work align with those broadly recognized in autonomous robotics and learning-from-human-feedback research. We view this contribution as a step toward safer and more dependable robotic learning systems, emphasizing robustness as a foundational requirement for responsible deployment.

References

Abdelkareem, Y., Shehata, S., and Karray, F. Advances in preference-based reinforcement learning: A review. In *2022 IEEE international conference on systems, man, and cybernetics (SMC)*, pp. 2527–2532. IEEE, 2022.

An, G., Lee, J., Zuo, X., Kosaka, N., Kim, K.-M., and Song, H. O. Direct preference-based policy optimization without reward modeling. *Advances in Neural Information Processing Systems*, 36:70247–70266, 2023.

Azar, M. G., Rowland, M., Piot, B., Guo, D., Calandriello, D., Valko, M., and Munos, R. A general theoretical paradigm to understand learning from human preferences, 2023. URL <https://arxiv.org/abs/2310.12036>.

Azar, M. G., Guo, Z. D., Piot, B., Munos, R., Rowland, M., Valko, M., and Calandriello, D. A general theoretical paradigm to understand learning from human preferences. In *International Conference on Artificial Intelligence and Statistics*, pp. 4447–4455. PMLR, 2024.

Black, K., Janner, M., Du, Y., Kostrikov, I., and Levine, S. Training diffusion models with reinforcement learning. *ArXiv*, abs/2305.13301, 2023. URL <https://api.semanticscholar.org/CorpusID:258833251>.

Black, K., Janner, M., Du, Y., Kostrikov, I., and Levine, S. Training diffusion models with reinforcement learning, 2024. URL <https://arxiv.org/abs/2305.13301>.

Bradley, R. A. and Terry, M. E. Rank analysis of incomplete block designs: I. the method of paired comparisons. *Biometrika*, 39(3/4):324–345, 1952.

Cao, X., Xu, Z., Guang, M., Long, K., Bakker, M. A., Wang, Y., and Yu, C. Latent collective preference optimization: A general framework for robust llm alignment. *arXiv e-prints*, pp. arXiv–2509, 2025.

Chen, Y., Jha, D. K., Tomizuka, M., and Romeres, D. FDPP: Fine-tune Diffusion Policy with Human Preference. *arXiv e-prints*, art. arXiv:2501.08259, January 2025. doi: 10.48550/arXiv.2501.08259.

Cheng, J., Xiong, G., Dai, X., Miao, Q., Lv, Y., and Wang, F.-Y. Rime: Robust preference-based reinforcement learning with noisy preferences. In *International Conference on Machine Learning*, pp. 8229–8247. PMLR, 2024.

Chi, C., Xu, Z., Feng, S., Cousineau, E., Du, Y., Burchfiel, B., Tedrake, R., and Song, S. Diffusion policy: Visuomotor policy learning via action diffusion. *The International Journal of Robotics Research*, 44(10-11):1684–1704, 2025.

Christiano, P. F., Leike, J., Brown, T., Martic, M., Legg, S., and Amodei, D. Deep reinforcement learning from human preferences. *Advances in neural information processing systems*, 30, 2017.

He, K., Zhang, X., Ren, S., and Sun, J. Deep residual learning for image recognition. In *Proceedings of the IEEE conference on computer vision and pattern recognition*, pp. 770–778, 2016.

Hejna, J. and Sadigh, D. Inverse preference learning: Preference-based rl without a reward function. *Advances in Neural Information Processing Systems*, 36:18806–18827, 2023.

Hejna, J., Rafailov, R., Sikchi, H., Finn, C., Niekum, S., Knox, W. B., and Sadigh, D. Contrastive preference learning: learning from human feedback without rl. *arXiv preprint arXiv:2310.13639*, 2023.

Hejna, J., Rafailov, R., Sikchi, H., Finn, C., Niekum, S., Knox, W. B., and Sadigh, D. Contrastive preference learning: Learning from human feedback without reinforcement learning. In *The Twelfth International Conference on Learning Representations*, 2024. URL <https://openreview.net/forum?id=iX1RjVQODj>.

Heo, J., Lee, Y. J., Kim, J., Kwak, M. G., Park, Y. J., and Kim, S. B. Mixing corrupted preferences for robust and feedback-efficient preference-based reinforcement learning. *Knowledge-Based Systems*, 309:112824, 2025.

Ho, J., Jain, A., and Abbeel, P. Denoising diffusion probabilistic models. *Advances in neural information processing systems*, 33:6840–6851, 2020.

Huang, S., Levy, M., Gupta, A., Ekpo, D., Zheng, R., and Shrivastava, A. Trend: Tri-teaching for robust preference-based reinforcement learning with demonstrations. *arXiv preprint arXiv:2505.06079*, 2025.

Jia, X., Blessing, D., Jiang, X., Reuss, M., Donat, A., Loutikov, R., and Neumann, G. Towards diverse behaviors: A benchmark for imitation learning with human demonstrations. In *The Twelfth International Conference on Learning Representations*, 2024. URL <https://openreview.net/forum?id=6pPYRXKPpw>.

Jin, W., Murphey, T. D., Lu, Z., and Mou, S. Learning from human directional corrections. *IEEE Transactions on Robotics*, 39(1):625–644, 2022.

Kim, C. W., Verma, S., Tec, M., and Tambe, M. Lightweight robust direct preference optimization. *arXiv preprint arXiv:2510.23590*, 2025.

Knox, W. B., Hatgis-Kessell, S., Adalgeirsson, S. O., Booth, S., Dragan, A., Stone, P., and Niekum, S. Learning optimal advantage from preferences and mistaking it for reward. In *Proceedings of the AAAI Conference on Artificial Intelligence*, volume 38, pp. 10066–10073, 2024.

Lee, K., Smith, L., Dragan, A., and Abbeel, P. B-pref: Benchmarking preference-based reinforcement learning. *arXiv preprint arXiv:2111.03026*, 2021a.

Lee, K., Smith, L. M., and Abbeel, P. Pebble: Feedback-efficient interactive reinforcement learning via relabeling experience and unsupervised pre-training. In Meila, M. and Zhang, T. (eds.), *Proceedings of the 38th International Conference on Machine Learning*, volume 139 of *Proceedings of Machine Learning Research*, pp. 6152–6163. PMLR, 18–24 Jul 2021b.

Li, Y., Das, S., and Taylor, M. E. Candere-coach: Reinforcement learning from noisy feedback. *arXiv preprint arXiv:2409.15521*, 2024.

Liang, X., Shu, K., Lee, K., and Abbeel, P. Reward uncertainty for exploration in preference-based reinforcement learning. In *International Conference on Learning Representations*, 2022. URL <https://openreview.net/forum?id=OWZVD-1-ZrC>.

Liu, R., Bai, F., Du, Y., and Yang, Y. Meta-reward-net: Implicitly differentiable reward learning for preference-based reinforcement learning. *Advances in Neural Information Processing Systems*, 35:22270–22284, 2022.

Luu, T. M., Lee, D., Lee, Y., and Yoo, C. D. Policy learning from large vision-language model feedback without reward modeling. *arXiv preprint arXiv:2507.23391*, 2025.

Ma, H., Chen, T., Wang, K., Li, N., and Dai, B. Efficient online reinforcement learning for diffusion policy. *arXiv preprint arXiv:2502.00361*, 2025.

Meng, Y., Xia, M., and Chen, D. Simpo: Simple preference optimization with a reference-free reward. *Advances in Neural Information Processing Systems*, 37:124198–124235, 2024a.

Meng, Y., Xia, M., and Chen, D. Simpo: Simple preference optimization with a reference-free reward, 2024b. URL <https://arxiv.org/abs/2405.14734>.

Park, J., Seo, Y., Shin, J., Lee, H., Abbeel, P., and Lee, K. Surf: Semi-supervised reward learning with data augmentation for feedback-efficient preference-based reinforcement learning. *arXiv preprint arXiv:2203.10050*, 2022.

Peng, X. B., Kumar, A., Zhang, G., and Levine, S. Advantage-weighted regression: Simple and scalable off-policy reinforcement learning. *arXiv preprint arXiv:1910.00177*, 2019.

Peters, J. and Schaal, S. Reinforcement learning by reward-weighted regression for operational space control. In *Proceedings of the 24th international conference on Machine learning*, pp. 745–750, 2007.

Plackett, R. L. The analysis of permutations. *Journal of the Royal Statistical Society Series C: Applied Statistics*, 24(2):193–202, 1975.

Rafailov, R., Sharma, A., Mitchell, E., Manning, C. D., Ermon, S., and Finn, C. Direct preference optimization: Your language model is secretly a reward model. *Advances in neural information processing systems*, 36:53728–53741, 2023.

Ramesh, S. S., Hu, Y., Chaimalas, I., Mehta, V., Sessa, P. G., Bou Ammar, H., and Bogunovic, I. Group robust preference optimization in reward-free rlhf. *Advances in Neural Information Processing Systems*, 37:37100–37137, 2024.

Ren, A. Z., Lidard, J., Ankile, L. L., Simeonov, A., Agrawal, P., Majumdar, A., Burchfiel, B., Dai, H., and Simchowitz, M. Diffusion policy policy optimization, 2024. URL <https://arxiv.org/abs/2409.00588>.

Seneviratne, G., An, J., Ellahy, S., Weerakoon, K., Elnoor, M. B., Kannan, J. D., Sunil, A. T., and Manocha, D. Halo: Human preference aligned offline reward learning for robot navigation. *arXiv preprint arXiv:2508.01539*, 2025.

Settles, B. *Active Learning*. Morgan & Claypool Publishers, 2012. ISBN 1608457257.

Shan, Z., Fan, C., Qiu, S., Shi, J., and Bai, C. Forward kl regularized preference optimization for aligning diffusion policies, 2024. URL <https://arxiv.org/abs/2409.05622>.

Tan, H., Chen, S., Xu, Y., Wang, Z., Ji, Y., Chi, C., Lyu, Y., Zhao, Z., Chen, X., Co, P., et al. Robo-dopamine: General process reward modeling for high-precision robotic manipulation. *arXiv preprint arXiv:2512.23703*, 2025.

Wolf, R., Shi, Y., Liu, S., and Rayyes, R. Diffusion models for robotic manipulation: A survey. *Frontiers in Robotics and AI*, 12:1606247, 2025.

Xia, W., Yang, Y., Wu, H., Ma, X., Kong, T., and Hu, D. Human-assisted robotic policy refinement via action preference optimization. In *The Thirty-ninth Annual Conference on Neural Information Processing Systems*.

Xie, Z., Zhang, H., Feng, Y., and Jin, W. Robust reward alignment via hypothesis space batch cutting. In *Forty-second International Conference on Machine Learning*, 2025. URL <https://openreview.net/forum?id=pL87Z7YTJS>.

Xu, H., Sharaf, A., Chen, Y., Tan, W., Shen, L., Durme, B. V., Murray, K., and Kim, Y. J. Contrastive preference optimization: Pushing the boundaries of llm performance in machine translation, 2024a. URL <https://arxiv.org/abs/2401.08417>.

Xu, H., Sharaf, A., Chen, Y., Tan, W., Shen, L., Van Durme, B., Murray, K., and Kim, Y. J. Contrastive preference optimization: Pushing the boundaries of llm performance in machine translation. *arXiv preprint arXiv:2401.08417*, 2024b.

Xue, H., Ren, J., Chen, W., Zhang, G., Fang, Y., Gu, G., Xu, H., and Lu, C. Reactive diffusion policy: Slow-fast visual-tactile policy learning for contact-rich manipulation. *arXiv preprint arXiv:2503.02881*, 2025.

Xue, W., An, B., Yan, S., and Xu, Z. Reinforcement learning from diverse human preferences. In *Proceedings of the Thirty-Third International Joint Conference on Artificial Intelligence, IJCAI '24*, 2024. ISBN 978-1-956792-04-1. doi: 10.24963/ijcai.2024/586. URL <https://doi.org/10.24963/ijcai.2024/586>.

Yang, K., Tao, J., Lyu, J., Ge, C., Chen, J., Li, Q., Shen, W., Zhu, X., and Li, X. Using human feedback to fine-tune diffusion models without any reward model. *2024 IEEE/CVF Conference on Computer Vision and Pattern Recognition (CVPR)*, pp. 8941–8951, 2023. URL <https://api.semanticscholar.org/CorpusID:265352082>.

Yuan, M., Yu, T., Ge, W., Yao, X., Li, D., Wang, H., Chen, J., Li, B., Zhang, W., Zeng, W., et al. A survey of behavior foundation model: Next-generation whole-body control system of humanoid robots. *IEEE Transactions on Pattern Analysis and Machine Intelligence*, 2025.

Ze, Y., Zhang, G., Zhang, K., Hu, C., Wang, M., and Xu, H. 3d diffusion policy: Generalizable visuomotor policy learning via simple 3d representations. *arXiv preprint arXiv:2403.03954*, 2024.

Zhao, T. Z., Kumar, V., Levine, S., and Finn, C. Learning fine-grained bimanual manipulation with low-cost hardware. *arXiv preprint arXiv:2304.13705*, 2023.

A. Proof of Lemmas

A.1. Proof of Lemma 4.1

Proof. (21) reaches the maximum value N if and only if $\theta \in \Theta \cap \bigcap_{i=1}^N \mathcal{C}_i \subseteq \mathcal{C}_j$, since all of the votes $V_{\mathcal{C}_i}(\theta), i = 1, \dots, N$ is 1. Thus the solution set to (21) is $\Theta \cap \bigcap_{i=1}^N \mathcal{C}_i \subseteq \mathcal{C}_j$. In noise-free case, combining the definition of θ^H and the cuts \mathcal{C}_i in (17). It is clear that $\theta^H \in \mathcal{C}_i, i = 1, \dots, N$. Combining with $\theta^H \in \Theta$, we have (21).

If the j -th preference pair is falsely labelled, the j -th cut \mathcal{C}_j is defined as:

$$\mathcal{C}_j = \left\{ \theta \in \Theta \mid \Delta Q_\theta(\mathbf{a}_{j,w}^+ | \mathbf{s}_j^+, \mathbf{a}_{j,l}^+ | \mathbf{s}_j^+) \geq 0 \right\}. \quad (25)$$

By the definition of θ^H , $\Delta Q_{\theta^H}(\mathbf{a}_{j,w}^+ | \mathbf{s}_j^+, \mathbf{a}_{j,l}^+ | \mathbf{s}_j^+) = \Delta Q(\mathbf{a}_{j,w}^+ | \mathbf{s}_j^+, \mathbf{a}_{j,l}^+ | \mathbf{s}_j^+) < 0$. We have $\theta^H \notin \mathcal{C}_j$ and therefore $\theta^H \notin \Theta \cap \bigcap_{i=1}^N \mathcal{C}_i$. In other words, θ^H cannot be found in the above solution set. \square

A.2. Proof of Lemma 4.2

Proof. With the definition of γ , there are at most $\lceil \gamma N \rceil$ incorrect labels and at least $\lfloor (1-\gamma)N \rfloor$ correct labels in the dataset. As a result, for θ^H , there will be at least $\lfloor (1-\gamma)N \rfloor$ votes, i.e., $\sum_{i=1}^N V_{\mathcal{C}_i}(\theta^H) \geq \lfloor (1-\gamma)N \rfloor$ and $H\left(\sum_{i=1}^N V_{\mathcal{C}_i}(\theta^H) - \lfloor (1-\gamma)N \rfloor + 0.5\right) = 1$, which means θ^H falls in the solution set in (22). \square

B. Experiment Setup Details

B.1. Task Details

1) Avoid (State-Based)

The robot must navigate to a green finish line while avoiding six static obstacles.

- **Observation:** 4-dimensional state (end-effector position and desired goal).
- **Modes & Preference:** The pretrained policy exhibits multimodal behavior, passing obstacles from either the *left* or *right*.

2) Pushing (State-Based)

The robot must push two blocks (red and green) into their corresponding target zones.

- **Observation:** 10-dimensional state (end-effector pose, block positions, block orientations).
- **Modes & Preference:** The task allows for diverse sorting order: **Green Block to Green Position or Red Block to Red Position**.

3) Sorting (State-Based)

The robot must sort one red block and one blue block into their matching target boxes.

- **Observation:** $(4 + 3X)$ -dimensional state where $X = 2$ blocks.
- **Preference:** We enforce a temporal preference, defining the sorting sequence: **Red block then Blue block or Blue Block then Red Block**.

4) Reorientation (Image-Based)

The robot must push a hollow box to a predefined target position and orientation.

- **Observation:** The policy conditions on two 96×96 RGB images (Front View + In-Hand View) along with the robot's proprioceptive state.
- **Preference:** The box can be pushed from the *inside* or *outside*.

5) Stacking (Image-Based)

The robot must stack three colored blocks (Red, Green, Blue) into a tower.

- **Observation:** Conditions on two 96×96 RGB images (Front View + In-Hand View) and proprioceptive state.
- **Preference:** With six possible stacking permutations, we select the order **Red** → **Blue** → **Green** and **Green** → **Blue** → **Red** for preference labelling.

B.2. Policy Architectures

- **State-Based UNet:** For *Avoid* and *Pushing*, we employ the standard Conditional UNet architecture (Chi et al., 2025). The model takes a history of observations ($T_{\text{obs}} = 2$) and predicts future action chunk of length ($T_{\text{pred}} = 16$).
- **Transformer ACT:** For *Sorting* and *Stacking*, we use the Action Chunking Transformer (ACT) architecture (Zhao et al., 2023). This model processes the observation history ($T_{\text{obs}} = 5$) and generate action chunk ($T_{\text{pred}} = 16$). For image observation, visual features from two camera views are extracted with ResNet-18 encoders (He et al., 2016) and are concatenated with robot’s proprioceptive state.
- **Image-Based MLP:** For *Aligning*, we employ a Single-Action diffusion architecture. Visual features from two camera views are extracted with ResNet-18 encoders and concatenated with the robot’s proprioceptive state. The model takes as input the current observation ($T_{\text{obs}} = 1$) to predict a single next action ($T_{\text{pred}} = 1$).

B.3. Training settings

For pretraining of policies, we used the same parameters, given in the D3IL benchmark repository.

Table 4. **Training Hyperparameters** Summary of key parameters used across different tasks.

| Parameter | Avoid | Pushing | Sorting | Aligning | Stacking |
|------------------------------|--------------------|--------------------|--------------------|--------------------|--------------------|
| Denoising Steps (K) | 20 | 20 | 16 | 4 | 16 |
| Optimizer | Adam | Adam | AdamW | AdamW | AdamW |
| Learning Rate | 3×10^{-5} | 3×10^{-5} | 1×10^{-5} | 1×10^{-5} | 1×10^{-5} |
| Batch Size | 64 | 64 | 64 | 32 | 32 |
| KL Coefficient (β) | 0.1 | 0.1 | 0.005 | 0.005 | 0.005 |
| Robustness Temp (α) | 1.0 | 1.0 | 1.0 | 1.0 | 1.0 |

B.4. Task Specific Parameters

The parameters N_{win} , N_{lose} and number of trials in evaluation is shown in Table 5.

Table 5. **Dataset and Evaluation Statistics.** Number of winner and loser trajectories collected for preference finetuning, along with the number of evaluation rollouts used to compute success and alignment rates.

| Task | # Winners N_{win} | # Losers N_{lose} | # Eval. Rollouts |
|----------|----------------------------|----------------------------|------------------|
| Avoid | 20 | 20 | 100 |
| Pushing | 30 | 30 | 100 |
| Sorting | 50 | 50 | 50 |
| Aligning | 40 | 40 | 20 |
| Stacking | 31 | 65 | 20 |

C. Additional Results

We conduct additional experiments by extending the noise level up to 0.95 on the pushing task. Representative evaluation trajectories are shown in Fig. 9. The results indicate that RoDiF maintains strong performance even when the corruption rate

approaches 0.45. When the noise level exceeds 0.5, the aligned mode flips, which is expected since the dominant preference label is reversed.

We additionally visualize the robot end-effector trajectories for the avoidance task, comparing the performance of DP-DPO and RoDiF under preference noise. The results, shown in Fig. 10, clearly demonstrate that RoDiF better preserves the preferred behavior mode under high noise levels.

The visualization of the policy rollouts with 10 preference pairs is shown in Fig. 11.

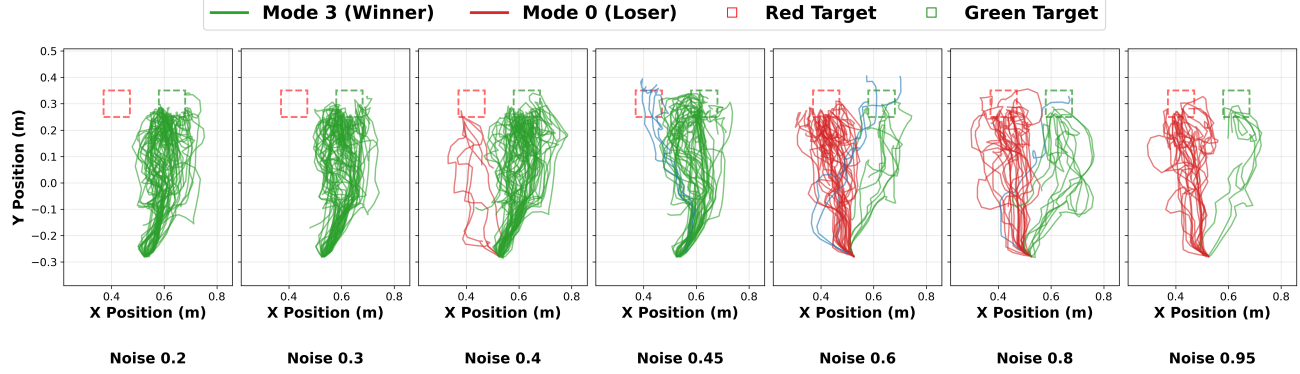


Figure 9. Mode visualization of the fine-tuned policies under different corruption rates. The regularization parameter γ was set as follows: $\gamma = 0.25$ for 20% noise, $\gamma = 0.35$ for 30% noise, $\gamma = 0.45$ for 40% noise, $\gamma = 0.5$ for 45% noise, $\gamma = 0.65$ for 60% noise, $\gamma = 0.85$ for 80% noise, and $\gamma = 0.95$ for 95% noise.

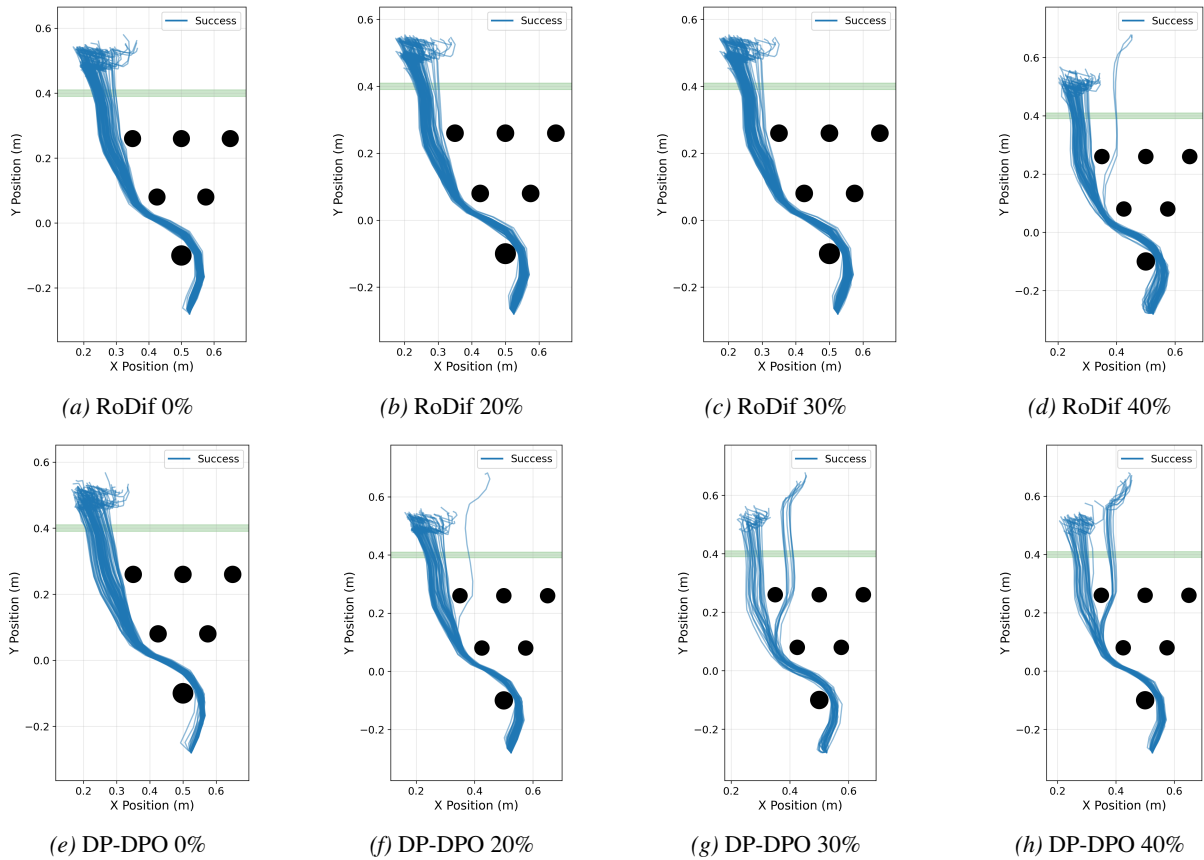


Figure 10. Mode visualization of the fine-tuned policy using RoDif and DP-DPO (15) across different corruption rate for Avoid Task. Avoid from left mode was selected as winner mode for fine-tuning. DP-DPO consists of loser modes even after fine-tuning the pretrained policy at different noise levels.

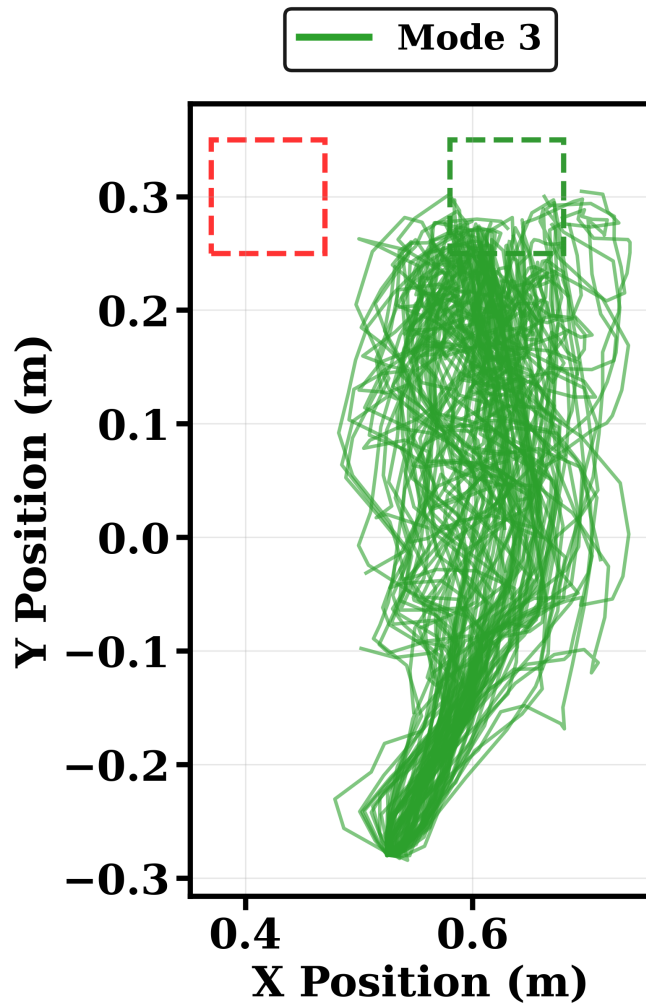


Figure 11. 10 Winner and 10 Loser fine-tuning. Mode 3 i.e. pushing green block to green position was selected as winner mode for fine-tuning.